Supplementary Information

Constructing sponge-like structured molecularly imprinted composite membranes for acteoside separation

Yuchen Ma, Chen Chen, Qingxin Wu, Guoqing Yang, Haojie Li*

State Key Laboratory Incubation Base for School of Chemistry and Chemical Engineering/State Key Laboratory Incubation Base for Green Processing of Chemical Engineering, Shihezi University, Shihezi 832003, Xinjiang, China

*: Corresponding author: Haojie Li

Email address: llihaojie@shzu.edu.cn

S1. Materials and Characterization.

Tetrapropyl orthosilicate, resorcinol, formaldehyde, and 2,2-dimethoxy-2-phenylacetophenone (DMPA, 99%) were purchased from Adamas Reagent Co., Ltd. (Shanghai, China). Polyvinylidene fluoride (PVDF, Mw: 400000) powder, polyvinylpyrrolidone (PVP, Mw: 58000), N-methyl-2-pyrrolidone (NMP, 99%), and potassium hydroxide were supplied by Shanghai McLean Biochemical Technology Co., Ltd. Ethanol, methanol, and ammonia hydroxide were purchased from Yongsheng Fine Chemical Co., Ltd. Acrylamide (AM, 98%) and methacrylic acid (MAA, 98%) were obtained from Aladdin Biochemical Technology Co., Ltd. (Shanghai, China). Nitrogen gas was supplied by Shanghai Weichuang Gas Co., Ltd. acteoside (ACT) and Echinacoside (ECH)were purchased from Chengdu Durst Biotechnology Co., Ltd.

The performance of SMICMs and NIMs was analyzed using high-performance liquid chromatography (HPLC).The surface microstructure and composition of PVDF, HMCs@PVDF, and SMICMs were characterized using scanning electron microscopy (SEM, SU8010, Hitachi, Japan). The micro-morphology of the filler HMCs was examined by transmission electron microscopy (TEM, JEM-2100F, JEOL, Japan). The specific surface area, pore size distribution, and pore size of HMCs were determined using a fully automated specific surface area and pore size analyzer (BET, BSD-660, Beishide Instrument Technology Co., Ltd., China). The HMCs functional groups on the SMICMs imprinted layer and the chemical bond changes before and after ACT adsorption were analyzed by Fourier transform infrared spectroscopy (FT-IR, Nicolet iS5, Thermo Scientific, USA) over a scanning range of 500–4000 cm^{-1} with a resolution of 1 cm^{-1}. The surface elemental composition and bonding states of CMICMs before and after adsorption were characterized using X-ray photoelectron spectroscopy (XPS, K-Alpha, Thermo Scientific, USA). The surface topography of SMICMs was analyzed by atomic force microscopy (AFM, Dimension ICON, Bruker, Germany). The hydrophilicity of PVDF, HMCs@PVDF, and SMICMs was evaluated using a water contact angle goniometer (WCA, OCA25, dataphysics, Germany). The tensile strength of PVDF (40×10×0.1 cm), HMCs@PVDF (40×10×0.12 cm), and SMICMs (40×10×0.12 cm) was tested using a universal testing machine (UTM, WDW-5B, Wenteng Testing Instrument Co., Ltd., China).

S2. The detailed operating conditions of HPLC

A Symmetry C18 column (250 × 4.6 mm, 5 μm, reversed-phase) was used to detect and separate the Agilent fluid system. The mobile phases were acetonitrile (A) and acetic acid/water (1:44, v/v) (B) with a flow rate of 1.0 mL/min and a detection time of 40 min. The detection temperature of the column oven was 30°C. The detection wavelength of the ultraviolet detector was 330 nm. All samples were examined using retention time and compared to the standard's UV-Vis spectrum.

S3. Adsorption isotherms experiments

SMICMs and NIMs were equilibrated in 20 mL ACT solutions spanning multiple concentrations at 30°C for 24 hours. Triplicate trials were conducted for each condition. HPLC quantified ACT concentrations pre- and post-adsorption. The equilibrium adsorption capacity (Q_e, mg·g^{-1}) was computed using Eq.1:

$$Q_e = \frac{(C_0 - C_e) \times V}{m} \tag{S-1}$$

Within these models, C_0 and C_e (mg/mL) signify the initial and equilibrium ACT concentrations in solution, respectively. ACT adsorption isotherms, describing the relationship between solution concentration and adsorbed amount, were modeled using the Langmuir and Freundlich equations (S-2,S-3). V (mL) denotes the solution volume, while m (g) represents the mass of the adsorbent membrane. The Langmuir model employs parameters Q_m (mg/g), the theoretical maximum adsorption capacity, and K_L, an adsorption constant. The Freundlich model is characterized by its constant K_F and the dimensionless exponent n.

$$Q_e = \frac{K_L Q_m C_e}{1 + K_L C_e} \tag{S-2}$$

$$Q_e = K_F C_e^{\frac{1}{n}} \tag{S-3}$$

In the adsorption models, K_L and K_F correspond to the Langmuir and Freundlich equilibrium constants, respectively. The term n signifies a unitless Freundlich affinity coefficient, while Q_e ($mg\cdot g^{-1}$) designates the experimental equilibrium adsorption capacity and Q_m ($mg\cdot g^{-1}$) the modeled maximum adsorption capacity.

S4. Adsorption kinetics experiments

A SMICMs or NINMs sample was immersed in 20 mL of 0.6 mg/mL ACT solution (HPLC purity ≥50%, 30°C). ACT concentrations at designated time intervals were measured by HPLC. Qt (mg/g) was calculated using S-4 with triplicate tests:

$$Q_t = \frac{(C_0 - C_t) \times V}{m} \tag{S-4}$$

where C_t (mg/mL) denotes the ACT concentration at binding time t.The kinetics of ACT binding were evaluated by applying the pseudo-first-order (S-5) and pseudo-second-order (S-6) kinetic models.

$$Q_t = Q_e - Q_e e^{-K_1 t} \tag{S-5}$$

$$Q_t = \frac{K_2 Q_e^2 t}{1 + K_2 Q_t t} \tag{S-6}$$

Within these kinetic models, Q_e (mg/g) characterizes the adsorbed amount of ACT at equilibrium for both SMICMs and NIMs, while t (min) signifies the contact duration. The constant $K1$ (min^{-1}) corresponds to the pseudo-first-order rate, and $K2$ ($g \cdot mg^{-1} \cdot min^{-1}$) represents the rate constant for the pseudo-second-order model.

S5. Selectivity experiments

In order to investigate selectivity of the SMICMs, a mixture solution of different concentrations containing ACT and ECH were prepared by using the standard solutions. For the selectivity tests, one piece of SMICMs was immersed into 20 mL of the stock solutions, and the stock solutions was shaken at 30°C for 24 h. The residual molecules in the stock solutions were examined by HPLC, the whole selective rebinding experiments were conducted in triplicate.

The selective rebinding experiments were performed to evaluate the selectivity of SMICMs and NIMs for ACT. It was carried out in a mixed solution of ACT and ECH (20 mL, 0.5 mg/mL). A piece of SMICMs put into the mixed solution, and the solution was oscillated at 30°C for 24 h. Then the ACT or ECH in the solution was detected by HPLC. The relevant parameters of the distribution coefficient (K_D, L/g), selectivity factor (K), and relative selectivity factor (α) were calculated by equations (S-7) - (S-9).

$$K_D = \frac{Q_e}{M \times C_e} \tag{S-7}$$

$$K = \frac{K_{D(ACT)}}{K_{D(ECH)}} \tag{S-8}$$

$$\alpha = \frac{K_{MICMNs}}{K_{NINMs}} \tag{S-9}$$

where C_e (mg/mL) represented equilibrium concentration of ACT after rebinding. Q_e (mg/g) represented equilibrium rebinding capacity of SMICMs, and M (mg) was the weight of SMICMs.

S6. The detailed regeneration tests

For the recycled adsorption-desorption experiments, a piece of SMICMs suspended in the ACT (HPLC⩾50%) stock solution (20 mL, 0.8 mg/mL) to reach the adsorption equilibrium. After rebinding, the saturated-adsorbed SMICMs were adequately rinsed by the methanol/acetic acid (9:1, v/v) to remove ACT templates until no ACT could be detected in the eluent, the membranes were then washed with ultrapure water many times. The regenerated SMICMs were reused for another adsorption-desorption cycle, and this adsorption-desorption cycle would be repeated for 10 times. Then, rebinding capacities and regeneration rates of regenerated SMICMs after each cycle were calculated respectively.

S7. Permselectivity experiments

Permselectivity characterization proved essential for assessing membrane functionality and elucidating transport mechanisms. Permeation experiments utilized a custom H-configuration glass cell. As a critical indicator of SMICM separation efficacy, permselectivity data provide mechanistic validation for selective transport processes. Membrane permeability coefficients were calculated using the following equations:

$$J_x = \frac{\Delta C_x V}{\Delta t\, A} \qquad x = ACT\ and\ ECH \tag{S-10}$$

$$P = \frac{J_x d}{(C_{Fx} - C_{Rx})} \qquad x = ACT\ and\ ECH \tag{S-11}$$

$$\beta_{i/j} = \frac{P_i}{P_j} \qquad i, j = ACT\ and\ ECH,\ SMICMs\ and\ NIMs \tag{S-12}$$

Within these calculations, A signifies the membrane's functional surface area (cm^2), d its thickness (cm), and V the liquid volume (mL) within either the donor or acceptor compartment. The term $\Delta C_x/\Delta t$ quantifies the temporal variation in solute concentration within the acceptor chamber. Conversely, $(C_{Fx} - C_{Rx})$ reflects the trans-membrane concentration gradient across the H-cell compartments.

S8. The permeate flux of membranes

The permeate flux for different membranes was determined by a vacuum suction filtration device, and the diameter of membrane was 3.4 cm. The vacuum suction filtration process lasted for 60 min at the vacuum degree of -0.1 MPa (the first cycle). Then, the filtration pressure was released to restore the filter membrane for 60 min, and the volume of water was measured. The above experimental process was repeated three times. The permeate flux of J ($L/(m^2{\cdot}h)$) were calculated by equation (S-13):

$$J = V/(A \times t) \tag{S-13}$$

where V (L) was permeation volume throughout the membrane, A (m^2) was membrane permeation area and t (h) was the permeate time.

Fig. S3 showed the permeation flux of the PVDF pristine membrane, HMCs@PVDF, MICMNs, and NIMs. As can be seen from Fig. S3, the permeation flux of HMCs@PVDF was consistently higher than that of the PVDF pristine membrane. In addition, compared with HMCs@PVDF, the permeation flux of SMICMs and NIMs was slightly reduced. These results were consistent with the porosity measurements. The results indicated that the incorporation of HMCs enhanced the permeability of the membrane. The increase in membrane permeation flux was beneficial for accelerating the separation of MICMNs for ACT.

S9. The anti-fouling tests and performance of membranes

The pure water flux of J_{w1} (L/(m^2·h)), the permeate flux of foulant solution (both ACT and ECH concentrations of 0.5 mg/mL) was calculated as J_p (L/(m^2·h)). The pure water flux of cleaned membranes (J_{w2}, (L/(m^2·h))) was measured again at 0.1 MPa. Subsequently, the membrane was immersed in deionized water. The flux recovery ratio (*FRR*), irreversible fouling ratio (R_{ir}), reversible fouling ratio (R_r), and total fouling ratio (R_t) were calculated by the equations (S-14) - (S-17):

$$FRR = J_{w2}/J_{w1} \times 100\% \tag{S-14}$$

$$R_{ir} = (1 - J_{w2}/J_{w1}) \times 100\% \tag{S-15}$$

$$R_r = (J_{w2} - J_p)/J_{w1} \times 100\% \tag{S-16}$$

$$R_t = (1 - J_p/J_{w1}) \times 100\% \tag{S-17}$$

In filtration test, the *FRR*, R_{ir}, R_r, R_t and were used to measure the anti-fouling performance. The specific data is shown in Table S2.

S10. Figure and table data

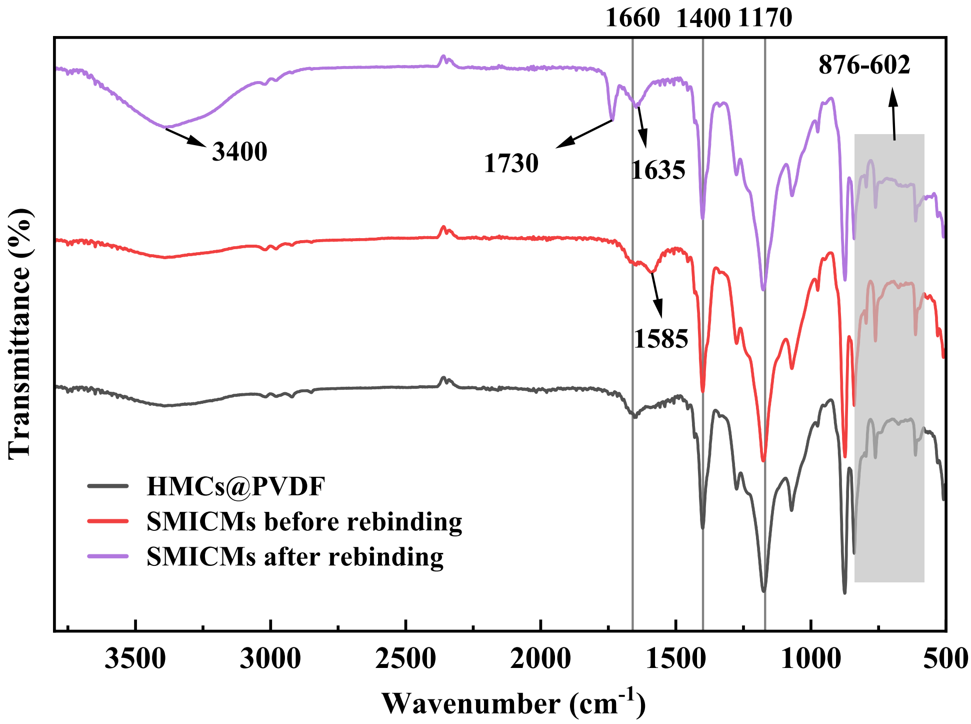

Fig. S1. FTIR spectra images of prepared membranes.

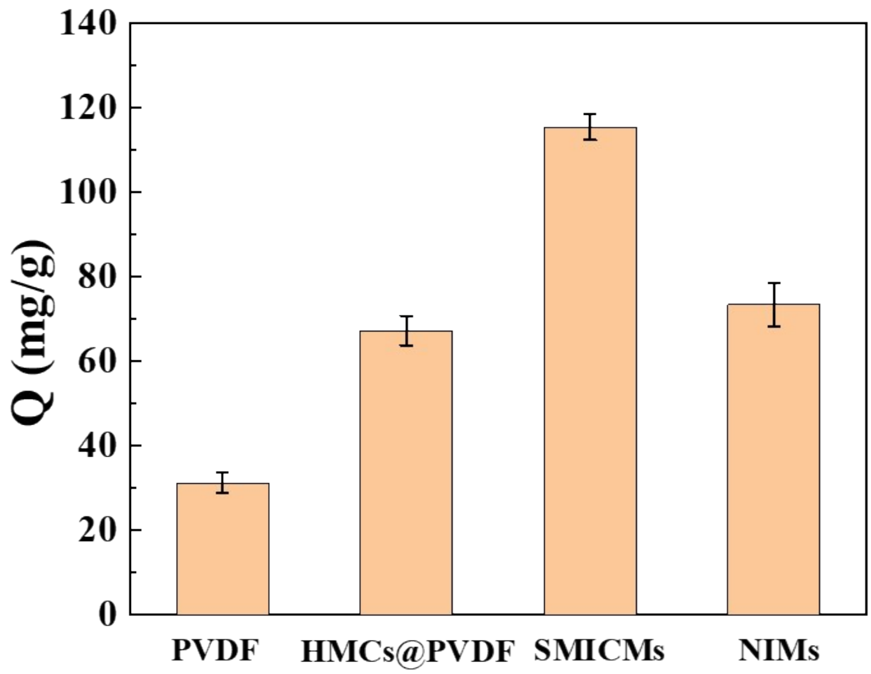

Fig. S2. Measurement of the adsorption capacity of ACT by different membranes

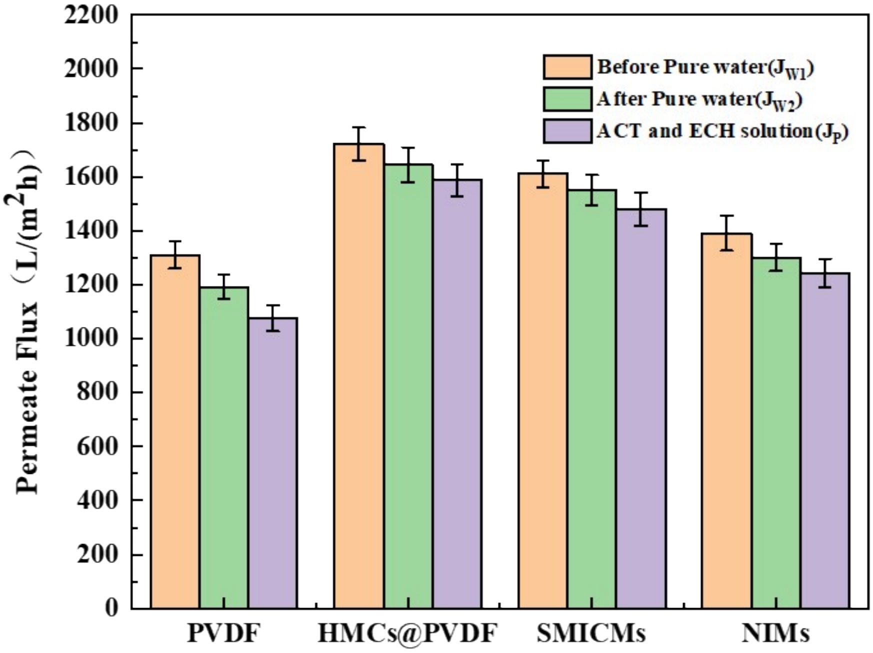

Fig. S3. The permeate flux of the PVDF pristine membrane, THP@PVDF, MICMNs and NIMs.

Table S1. Mechanical properties of PVDF pristine membranes, HMCs@PVDF, SMICMs and NIMs.

Membranes	Maximum strength (MPa)	Maximum elongation (%)	Young's modulus (MPa)
PVDF	2.778 ± 0.14	45.45 ±1.52	38.91 ± 3.17
HMCs@PVDF	3.51 ± 0.21	50.68 ±3.81	53.93 ± 5.35
SMICMs	3.84 ± 0.22	80.54 ±4.23	76.75 ± 5.54
NIMs	4.33 ± 0.11	70.94 ±3.11	67.31 ± 4.51

Table S2. The flux recovery ratio, irreversible fouling ratio, reversible fouling ratio, and total fouling ratio for the prepared membranes.

Membranes	FRR (%)	R_{ir} (%)	R_r (%)	R_t (%)
PVDF	92.31	6.34	2.32	8.68
HMCs@PVDF	96.32	3.68	2.81	6.54
SMICMs	95.82	4.16	4.62	8.69
NIMs	96.24	3.77	4.01	7.73

Table S3. Pseudo-first-order and pseudo-second-order kinetic adsorption constants of SMICMs and NIMs.

Membrane	$Q_{e,exp}$	Pseudo-first-order model			Pseudo-second-order model		
		$Q_{e,cal}$	K_1	R^2	$Q_{e,cal}$	K_2	R^2
SMICMs	189.40	181.81	0.0100	0.9721	205.06	0.682×10^{-4}	0.9991
NIMs	67.11	66.72	0.0002	0.9579	73.81	2.063×10^{-4}	0.9961

Table S4. Adsorption isothermal model parameters of SMICMs and NIMs.

Membrane	$Q_{e,exp}$	Langmuir model			Freundlich model			
		$Q_{e,cal}$	K_L	R^2	$Q_{e,cal}$	K_F	1/n	R^2
SMICMs	160.27	273.37	3.07	0.9959	223.58	207.97	0.4073	0.9493
NIMs	65.32	68.22	7.24	0.9986	64.20	61.16	0.2838	0.9241

Table S5. Time-dependent permeation data (10 h) for ACT and ECH in SMICMs and NIMs.

Membrane	Permeable molecule	J (mg·cm^{-2}·h^{-1})	P (cm^{-2}·h^{-1})	$\beta_{ECH/ACT}$
SMICMs	ACT	12.89×10^{-4}	2.02×10^{-2}	9.62
	ECH	123.81×10^{-4}	19.44×10^{-2}	
NIMs	ACT	110.85×10^{-4}	17.40×10^{-2}	1.00
	ECH	111.73×10^{-4}	17.54×10^{-2}	